Article

Not peer-reviewed version

A Study on the High-Temperature Molten Salt Corrosion Resistance of Hot-Dip Aluminum/Carburizing Composite Coating on Ti65 Titanium Alloy

Jiayi Wang and Faguo Li *

Posted Date: 19 June 2023

doi: 10.20944/preprints202306.1311.v1

Keywords: titanium alloy; hot-dip aluminum/carburizing composite coating; hot dip aluminum coating; molten salt corrosion

Article

A Study on the High-Temperature Molten Salt Corrosion Resistance of Hot-Dip Aluminum/Carburizing Composite Coating on Ti65 Titanium Alloy

Jiayi Wang and Faguo Li *

School of Materials Science and Engineering, Xiangtan University, Xiangtan, Hunan, China, 411105; Wjy19892011340@163.com (J.W.)

* Correspondence: lifaguo@xtu.edu.cn (F.L.)

Abstract: This paper presents a new method of preparing a coating on the Ti65 titanium alloy by a two-step procedure comprising hot-dipped aluminum and solid carburization. The effects of the carburization in the presence of NaCl deposit at 810°C have been systematically studied. In this article, the microstructure, morphology, phase composition of the coating, and the corrosion products were investigated by SEM, EDS, and X-ray diffraction. Results indicated that the corrosion resistance of hot dip aluminum/carburizing composite coating was not significantly enhanced by hot dip aluminum coating. This can be attributed to the formation of TiC and Ti_3AlC after carburization, which promoted the formation of loose and unprotected TiO_2 in the coating during molten salt corrosion. In addition, the oxidation of the carbon atom into CO_2 /CO leaded to a high concentration of vacancy in the coating, creating channels for NaCl to penetrate the coating and accelerated the corrosion rate.

Keywords: titanium alloy; hot-dip aluminum/carburizing composite coating; hot dip aluminum coating; molten salt corrosion

1. Introduction

Titanium alloys are widely recognized as ideal materials for compressor blades due to their excellent properties, such as low density, high strength, and strong corrosion resistance [1-5]. However, when applied in the marine environments, the titanium alloy surface accumulates salt sediment in the form of NaCl, resulting in the synergistic corrosion effects of elevated temperatures, Cl^- ions, and oxygen on the compressor components. Consequently, this leads to severe corrosion failures with significantly higher corrosion rates compared to oxidation rates under normal atmospheric conditions [6-9]. Extensive researchers have been conducted to investigate the mechanisms of resistance to hot corrosion of titanium alloy. Clément Ciszak et al. [6] highlighted the detrimental effect of NaCl deposits at high temperatures, leading to the establishment of an active corrosion phenomenon at the metal/oxide interface. Rui Li et al. [8] found a mixed corrosion mechanism involving both classic oxidation and active oxidation when exposed to NaCl solution spraying environments. According to the research of Z. Yao et al. [9]indicated that the reaction of the metal, oxygen, and deposited sodium chloride resulted in the formation of a non-protective scale and accelerated the oxidation of the alloy. Therefore, it's essential to develop suitable protective coatings for titanium alloy to enhance the resistance against oxidation and hot salt corrosion under high-temperature conditions.

According to previous research the application of protective surface coatings is a preferred way for enhancing the corrosion resistance of titanium alloys. These coatings provide additional protection by preventing contaminated salt from attacking the substrate [10, 11]. One promising coating technique for improving the hot corrosion resistance of titanium alloys is the preparation of

 doi:10.20944/preprints202306.1311.v1

aluminate coatings [12-14]. Among the various methods available for preparing aluminum coatings, hot-dip aluminizing has garnered significant attention from researchers due to its advantages, such as a simple preparation process, low cost, and excellent coating adherence [15-17]. In a study by Payank Pate et al. [18], the microstructure of the aluminized coating after diffusion heat treatments was found to consist of an outer layer of Al_2O_3, followed by $TiAl_3$ and $TiAl_2$ phases. Yuansheng Wang et al. [19] discovered the formation of $TiAl_3$, θ-Al_2O_3, and compact α-Al_2O_3 in the outer layer, which was believed to contribute to improved oxidation resistance at high temperatures. Shiang-Cheng Jeng [20] successfully prepared an aluminized Ti-6Al-4V alloy by hot-dipping aluminum under a protective argon atmosphere at 800 °C, and the results demonstrated that the aluminized coating provided significant protection against oxidation at this temperature.

The carburization process has been widely utilized in Ti-based alloys. Hong-Qiang DUAN [21]discovered that solid carburization on Ti-6Al-4V alloy and (TiB+La_2O_3)/Ti composite can enhance surface hardness. Cuijiao Liao et al. [22] observed the formation of a stable passivation film on TiAl alloy through solid carburizing, which improved the corrosion resistance of porous TiAl alloy. Tianhang Yao et al. [23]demonstrated that the carburization process is an effective and feasible treatment for enhancing the oxidation resistance of high Nb-containing TiAl alloys. However, limited research has been conducted on carburizing after aluminized titanium alloy coating, and the mechanism of this coating against molten salt corrosion remains not fully understood. Therefore, the objective of this study is to investigate the high-temperature molten salt corrosion resistance of the hot-dip aluminum/carburizing composite coating on Ti65 titanium alloy and systematically discuss the corrosion behavior mechanism.

2. Materials and Methods

2.1. Material preparation

Ti65 alloy was used as the substrate material. Before the experiments, specimens were cut into 15 mm × 10 mm × 3 mm pieces with a sparkline saw. To facilitate its hanging into molten aluminum, a hole of 3mm diameter was drilled near the edge of the samples. All the surfaces were ground with 400#, 600#, and 800# SiC paper and polished to achieve a mirror-like surface using aluminum oxide polishing.

Table 1. Chemical composition of the Ti65 alloy (wt%).

Al	Sn	Ta	W	Zr	Mo	Nd	Si	C	Ti
5.9	4.0	2.0	1.0	3.5	0.3	0.3	0.35	0.05	Bal.

2.2. Hot-dip alumininzing

Prior to the hot-dip aluminizing, the surface of the samples was first ultrasonically degreased with acetone for 3-5min and followed by rinsing in water. Subsequently, samples were pickled with ethanol solution ultrasonic agitation for 5-10 min and then were dried immediately. After the pre-cleaning process, the pure aluminum (Al >99.7 wt.%) was melted in a graphite crucible. The molten Al bath was maintained at a 760℃ well resistance furnace (Xiangtan Samsung Instrument Co., LTD, Xiangtan, China). The treated samples were vertically immersed into the aluminum melt bath under an argon atmosphere for 10min. When arrived the desired hot-dipping time was, the specimen was quickly extracted from the melt and shaken off the excess melt of its surface, and then air cooled to room temperature. The derived specimen was denoted as hot dip aluminum coating.

2.3. Solid carburization

 doi:10.20944/preprints202306.1311.v1

The hot dip aluminum alloy was buried in a corundum crucible. The composition of the used solid carburized was 10%Na_2CO_3-10%Ba_2CO_3-5%$CaCO_3$ and the charcoal (particle size 1.5–3 mm). After being covered with an alumina lid and sealed by silica sol binder, the crucible was put into the center of the muffle furnace chamber (Xiangtan Samsung Instrument Co., LTD, Xiangtan, China). Then the tests were conducted at 1050 °C using a furnace for 4h followed by furnace cooling. Finally, the samples with coatings were taken out from the crucible powder, cleaned, and dried for corrosion test. This coating was named hot dip aluminum/carburizing composite coating.

2.4. Corrosion experiments

Prior to the corrosion test, the sample was placed in absolute ethanol for ultrasonic cleaning. After cleaning, the samples were dried for 2 hours at 100 °C. The initial mass was subsequently measured on an electronic analytical balance with an accuracy of 0.0001 g, and the mass was tested three times and the average mass gain value is presented in this work. The corrosion weight change rate was calculated to assess the performance of molten salt corrosion resistance on the coated and uncoated specimens at high temperatures. The samples were buried in a powder consisting of solid NaCl in ceramic crucibles. The corrosion tests were started by introducing the crucible directly into the hot muffle furnace (Xiangtan Samsung Instrument Co., LTD, Xiangtan, China) at 810 °C in static air to ensure rapid heating-up. The reference samples without the coating but with salt deposits were prepared in the same way. After given intervals (5, 5, 5, 5, 5, 10, 10, 10, 31, 24h), the samples were removed from the furnace and cooled in the air to room temperature. Subsequently, the corroded samples were washed in boiling deionized water for 30 min to clean out the remaining unreacted salt completely and then dried completely. The mass of each sample was measured using an electronic balance. The mass gain per unit area after each cycle was calculated using Eq. 1:

$$\Delta w = (m_1 - m_0)/S \quad (1)$$

where m_1 represents the weight (mg) after each interval, m_0 represents the weight (mg) at the beginning of each cycle, and S is the total sample surface area (cm^2). In addition, for every experiment, three specimens were used in the same condition to get the average mass change.

2.5. Analytical characterization

The coatings were analyzed using X-ray diffraction (XRD) and scanning electron microscopy with energy disperse X-ray analysis (SEM/EDAX). X-ray diffractometer (Rigaku D/max 2500, Japan) with Cu-Kα (λ = 1.542 Å) was used to analyze the phase composition of the coating before and after annealing (2θ: 10°–90°, Scanning speed: 10.0000 deg./min, current: 40mA, voltage: 40 kV). The microstructure and element distribution of the coating were analyzed by scanning electron microscopy (ZEISS EVO MA10, Zeiss, Jena, Germany). Energy dispersive spectrometer ((OXFORD X-MAXN, Zeiss, Jena, Germany) was used for the microstructure study and semi-quantitative chemical analysis, respectively.

3. Results

3.1. The microstructures of the hot dip aluminum/carburizing composite coating

Figure 1(a) exhibits cross-sectional morphologies of hot dip aluminum/carburizing composite coated samples. It has clearly layered structures with a thickness of about 196 μm and consecutive layers that differ in composition. From the enlarged SEM image (Figure 1(b)), there were some micro-cracks appear in the coating. According to the elemental mappings in Figure 2, there was sufficient Al and Ti in the coating, while the C atom was dispersed in the coating, a thin and continuous oxide scale rich O was formed at the surface which indicated that the coating is partially oxidized during carburization.

Preprints (www.preprints.org) | NOT PEER-REVIEWED | Posted: 19 June 2023 doi:10.20944/preprints202306.1311.v1

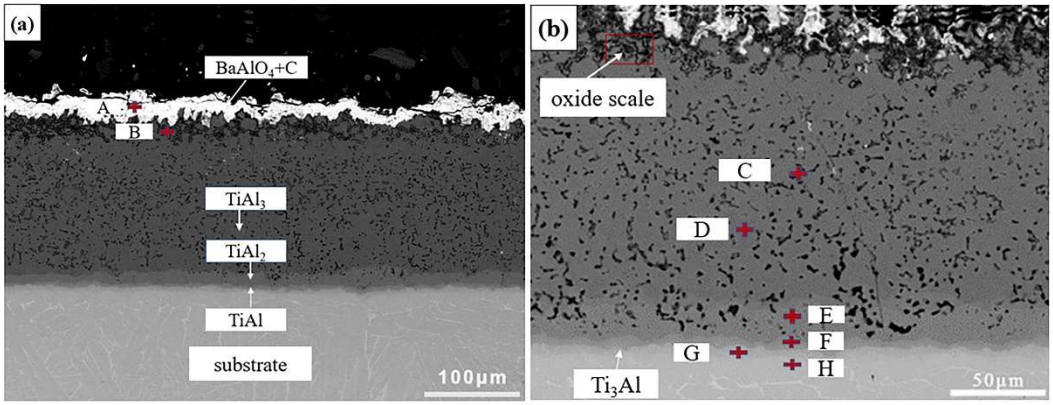

Figure 1. The cross-sectional morphologies of the hot dip aluminum/carburizing composite coating.

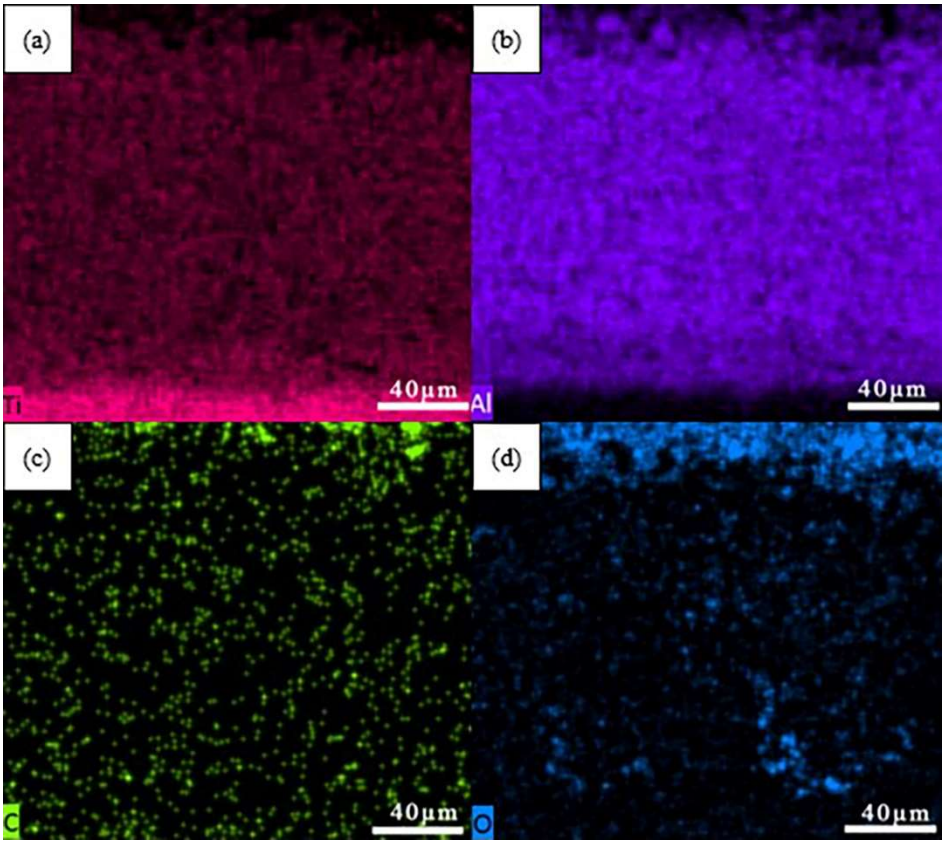

Figure 2. Element mappings of hot dip aluminum/carburizing composite coating (Ti, Al, C, and O are represented by red, purple, green, and blue respectively).

To further confirm the phase constitutions of the hot dip aluminum/carburizing composite coatings, the chemical compositions of layers were detected by EDS as listed in Table 2 and the XRD patterns are given in Figure 3. The EDS results indicated the chemical compositions of top scale (Point A in Figure 1(a) and Table 2) is 22.20C-51.20O-12.62Al-2.38Ti-11.51Ba (at.%). Combined with the XRD results, it is reasonable to assume that is $BaAlO_4$ produced by the reaction between the carburizing agent ($BaCO_3$) and Al atom, and some C atoms without reaction. The chemical composition of Point B in Figure 1(a) consists of a mixture of Al_2O_3,TiO_2, TiC, and Al_4C_3(15.31C-53.12O-24.72Al-6.85Ti, at%). In addition, some worm-like structure (Point C in Figure 1(b) and Table 2) was found in the coating. According to the EDS data in Table 2, it contains O element, but the content of the Ti element is very low, which is presumed to be composed of Al_2O_3 and Ti-Al. The reason for this structure maybe that the molten aluminum spreaded rapidly and Ti contacting molten aluminum began to

 doi:10.20944/preprints202306.1311.v1

dissolve and diffuse to the molten aluminum at the same time during the hot-dip aluminum. $TiAl_3$ is the first compound formed during the reaction between Ti and Al since the diffusion flux through $TiAl_3$ is several orders of magnitude higher than those through the other intermetallic compounds of the Ti-Al ($TiAl_2$, TiAl, Ti_3Al) [24]and the excess Al atoms would be expelled from the $TiAl_3$ crystal. With the nucleation and growth of $TiAl_3$ particles, the content of Al in the liquid phase gradually increased, and finally, all the Al changed into pure Al when reaching the freezing point. Therefore, granular $TiAl_3$ and pure Al filled between particles were formed after hot-dipped aluminum [19, 20, 25, 26]. During the carburizing process, the original pure Al is oxidized, and Al_2O_3 grains were generated into the coating as nucleating particles. With the extension of time, O atoms continued to enter the coating, and Al_2O_3 kept growing, and finally, all pure Al became Al_2O_3. Additionally, it can be seen that C atoms are dispersed at the liquid phase interface. Interestingly, it is found in the point D (Figure 1 (c) and Table 2) where the composition of Al to Ti is approximately to 3:1, illustrating that the the gray block was composed of $TiAl_3$ which is coincident with XRD patterns (Figure 3). It had been reported that the $TiAl_3$ phase is brittle in the aluminized coating to be a result of the cracks [18, 27]. Moreover, the coating near the substrate is still composed of titanium and aluminum in an atomic ratio of about 3:1, 1:1, 2:1, which would correspond to Ti_3Al, TiAl, and $TiAl_2$, respectively. Ti_3Al layer is compact and uniform and has good adhesion to the substrate. XRD pattern confirmed the existence of $TiAl_3$, Al_2O_3, and $TiAl_2$ phases, and a small amount of $TiAl_2$ peak was detected due to the oxidation of $TiAl_3$ to $TiAl_2$ during carburizing. Because the outer phase coating is so thick (~158μm), X-rays cannot reach the inner layer to detect TiAl and Ti_3Al, which agreed well with the XRD characterization.

Table 2. EDS results of regions marked in Figure 1 (at.%).

Point	Ti	Al	C	O	Ba	Possible Phase
A	2.38	12.62	22.20	51.20	11.51	$C+BaAlO_4$
B	6.85	24.72	15.31	53.12	/	$Al_2O_3+TiO_2+TiC+Al_4C_3$
C	15.94	60.62	/	25.45	/	Al_2O_3+Ti-Al
D	29.87	70.13	/	/	/	$TiAl_3$
E	33.19	66.81	/	/	/	$TiAl_2$
F	49.39	50.61	/	/	/	TiAl
G	70.52	29.48	/	/	/	Ti_3Al
H	83.71	16.29	/	/	/	Ti_3Al+Ti

Preprints (www.preprints.org) | NOT PEER-REVIEWED | Posted: 19 June 2023 doi:10.20944/preprints202306.1311.v1

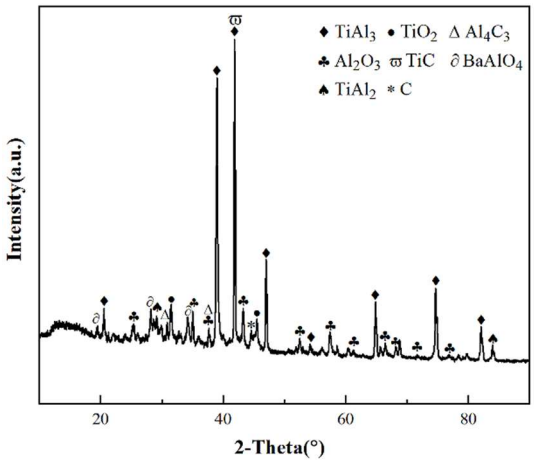

Figure 3. The XRD patterns of the hot dip aluminum/carburizing composite coating.

3.2. Molten salt corrosion kinetics

The evolution with time of the weight loss per unit area of Ti65 alloy, hot dip aluminum coating, and hot dip aluminum/carburizing composite coating after 120h molten salt corrosion test are presented in Figure 4. The data of the uncoated samples and hot dip aluminum coating are also given for comparison. Clearly, the weight loss of uncoated samples increased rapidly with the corrosion time extending due to the formation of the non-protective corrosion product at the surface. In contrast, hot dip aluminum coating and hot dip aluminum/carburizing composite coating alloy followed by a steady and smaller mass change. Additionally, the total mass loss of the hot dip aluminum coating and hot dip aluminum/carburizing composite alloy after 120 h of hot salt corrosion was near 0.67 mg/cm² and 5.06 mg/cm², respectively, while the total mass gains of uncoated alloys dramatically reduce to 76.57 mg/cm², which is approximately 114.5 and 15.1 times that of the hot dip aluminum coating and hot dip aluminum/carburizing composite coating. Therefore, the results indicate that the hot dip aluminum coating and hot dip aluminum/carburizing composite coating effectively decreased the molten salt corrosion rate of the Ti65 alloy.

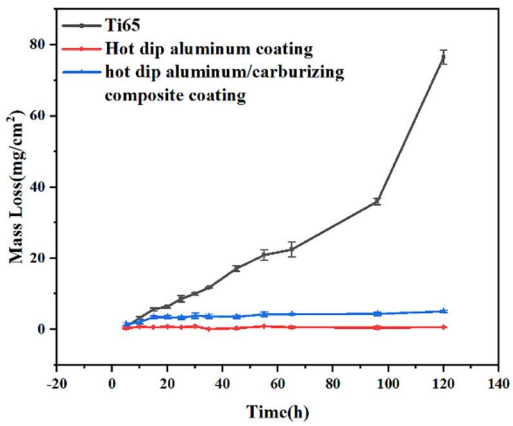

Figure 4. Kinetic curves of Ti65, hot dip aluminum coating and hot dip aluminum/carburizing composite coating.

3.3. Cross-sectional morphologies and surface analysis of hot dip aluminum coating after molten salt corrosion

After 120 hours of molten salt corrosion at 810°C, the surface observation results and XRD patterns of hot dip aluminum coating are shown in **Figure** 5 The surface of hot dip aluminum coating is peeled off and some irregular massive particles are scattered on the coating. The corrosion products detected on the surface of hot salt-corroded hot dip aluminum coating mainly consist of $TiAl_3$, and

Preprints (www.preprints.org) | NOT PEER-REVIEWED | Posted: 19 June 2023 doi:10.20944/preprints202306.1311.v1

only a small amount of diffraction peaks of Al_2O_3 and TiO_2 can be noticed in the XRD patterns, which confirm that the coating was stable under this condition.

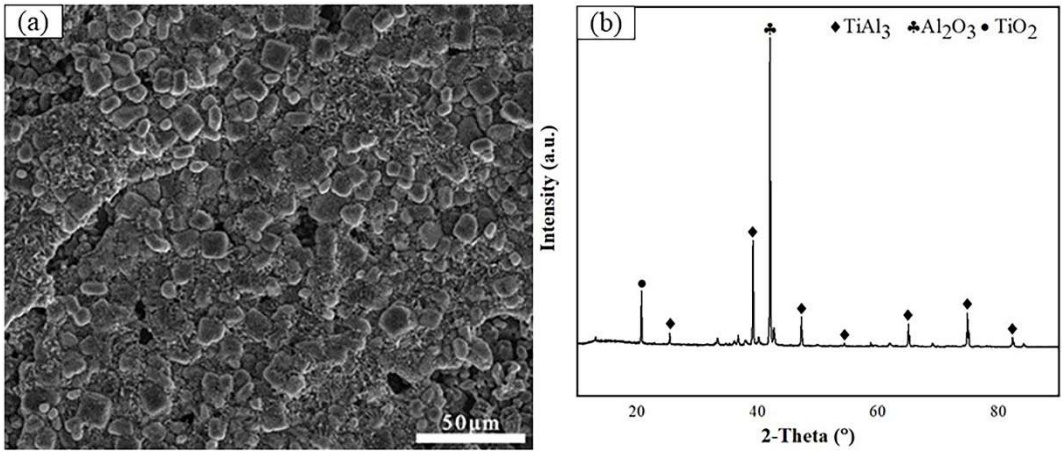

Figure 5. Surface morphologies(a) and XRD patterns (b) of hot dip aluminum coatings after corrosion in NaCl salt at 810 ◦C for 120 h.

Figure 6 depicts the cross-sectional morphologies of the aluminate coating. It is clear to observe a transverse crack throughout the coating due to the effect of thermal stress and molten salt oxidation. The worm-like structure of the corroded coating still appeared (Point A in Figure 6(b)). EDS results show that the element content at this point was 7.58Ti-38.41Al-54.01O (at. bal), suggesting that the phase composition was still Al_2O_3 and hot dip aluminum intermetallic compounds. The chemical composition of point B is 24.64Ti-55.54Al-31.34O phase, which may be composed of $TiAl_3$, Al_2O_3, and TiO_2 phases. The composition of points C, D, and E is 35.67Ti-64.33Al,51.78 Ti-48.22Al (at. bal), and 78.81Ti-21.19Al (at. bal), so it is reasonable to deduce that the phase is $TiAl_2$, TiAl, and Ti_3Al, respectively. The reason for the appearance of these three hot dip aluminum phases is that the Al and Ti atoms interdiffusion between the composite substrate and $TiAl_3$ coating with the extent of corrosion time. The formation of the transition diffusion layer of $TiAl_2$, TiAl, and Ti_3Al can reasonably reduce crack propagation or development, so the crack does not extend to the substrate.

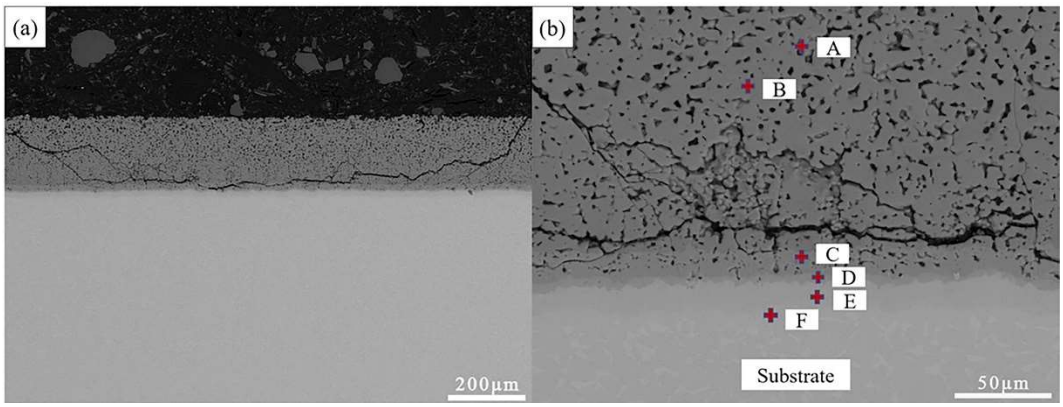

Figure 6. The cross-sectional morphologies of the hot dip aluminum coating in NaCl salt at 810 ◦C for 120h.

Table 3. EDS results of regions marked in Figure 6(b) (at.%).

Point	Ti	Al	O	Possible phase

Preprints (www.preprints.org) | NOT PEER-REVIEWED | Posted: 19 June 2023 doi:10.20944/preprints202306.1311.v1

A	7.58	38.41	54.01	Al_2O_3+Ti-Al
B	24.64	55.54	31.34	$TiAl_3$+Al_2O_3+TiO_2
C	35.67	64.33	/	$TiAl_2$
D	51.78	48.22	/	TiAl
E	78.81	21.19	/	Ti_3Al

3.4. Cross-sectional morphologies and surface analysis of hot dip aluminum/carburizing composite coatings after molten salt corrosion

Figure 7 demonstrates the surface morphology and XRD patterns of hot dip aluminum/carburizing composite coating after 120h of molten salt corrosion. It can be seen from Figure 7(a) that the surface was pretty rough with irregular-shape clusters dispersed and some region is composed of blocks that are separated by cracks. According to the XRD pattern (Figure 87(b)), it can be found that the main phase is the diffraction peak of Al_2O_3 and $TiAl_3$ phases, and the diffraction intensities of $TiAl_2$ and TiO_2 are enhanced. Besides, Al_4C_3 disappears but $NaAlO_4$, Na_2TiO_3, and TiAl newly emerge. XRD patterns inside the coating of samples after 5h and 120h of molten salt corrosion were conducted to further shed light on the microstructures of the hot dip aluminum/carburizing composite coatings (Figure 8). Ti_3AlC and Al_4C_3 X-ray diffraction peaks were found in the coating after 5h corrosion but disappeared in 120h, indicating that Ti_3AlC and Al_4C_3 were consumed by the reaction with the increment of exposure time. In addition, the TiAl phase was found in the samples corroded for 5h and 120h.

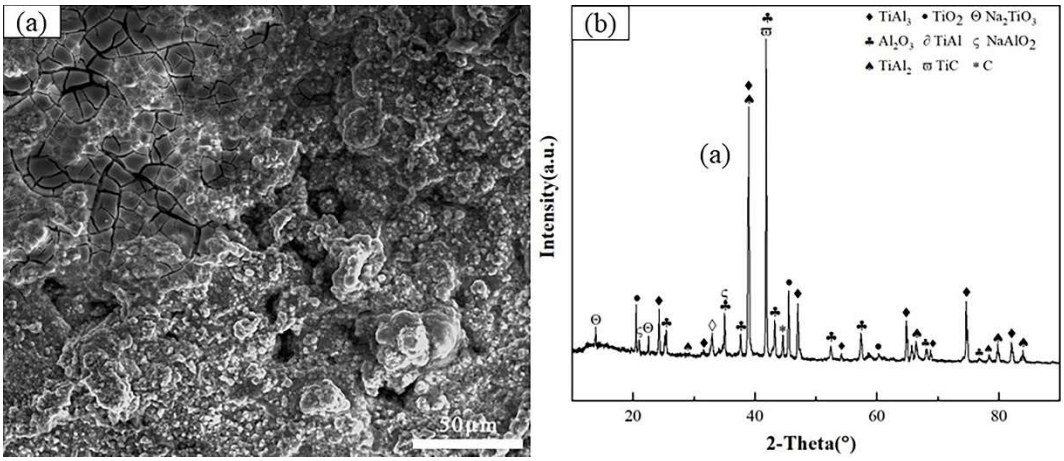

Figure 7. Surface morphologies(a) and XRD patterns (b) of hot dip aluminum coatings after corrosion in NaCl salt at 810 ◦C for 120 h.

Preprints (www.preprints.org) | NOT PEER-REVIEWED | Posted: 19 June 2023 doi:10.20944/preprints202306.1311.v1

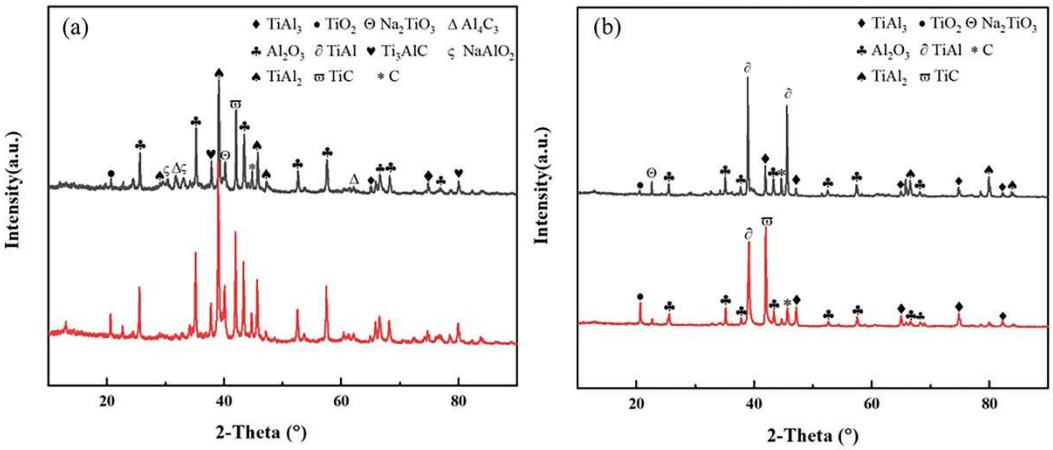

Figure 8. XRD patterns of hot dip aluminum/carburizing composite internal coatings after corrosion in NaCl salt at 810 ◦C for 5 h (a) and 120h (b), respectively.

Figure 9 depicts the cross-sectional morphology of the hot dip aluminum/carburizing composite coating covered by NaCl salt after 120h of hot corrosion at 810 ℃. It can be observed that the aluminum/carburizing composite coating suffered severe corrosion attack forming a thick, porous, and loose scale, whose characteristics are completely different from those of the non-corroded coating. Notably, the corrosion extent of hot dip aluminum/carburizing composite coating suffered a more severer corrosion attack than hot dip aluminum coating after exposure for the same period at the same temperature. In addition, there is no visible transverse penetrating crack observed. Combining EDS results and elemental mapping, the flocculent structure formed should be TiO_2 and Na_2TiO_3. TiO_2 mostly exist in loose island structure at high temperature, which is easy to flake and lead to the reduction of Ti content. The chemical composition of the dark part at the edge of the flocculent material is 9.5Ti-65.88Al-60.20O-0.64Cl-0.66Na, and the phase composition is $TiAl_3$ and Al_2O_3. Moreover, Point A (Figure 9(b)) and Point B (Figure 9(b)) with a similar chemical composition mainly composed of a mixed phase of Al_2O_3 and TiO_2 combined EDS analysis with its XRD pattern. Therefore, there was no protective barrier formed to prevent oxidation inside the coating. The gray block scale with the average content of Al and Ti 63.81 at% and 34.33 at%, respectively, was composed of $TiAl_2$ based on the EDS result. The coating near the base is still composed of TiAl and Ti_3Al. EDS elementary maps (Figure 10) reveal that both Cl and Na atoms have penetrated the coating successfully, and C atoms have not been detected.

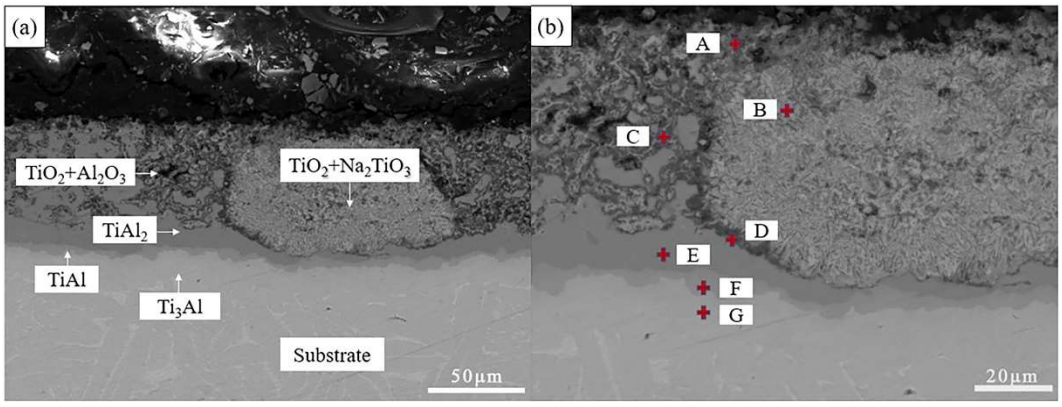

Figure 9. The cross-sectional morphologies of the hot dip aluminum/carburizing composite coatings in NaCl salt at 810 ◦C for 120h.

Preprints (www.preprints.org) | NOT PEER-REVIEWED | Posted: 19 June 2023 doi:10.20944/preprints202306.1311.v1

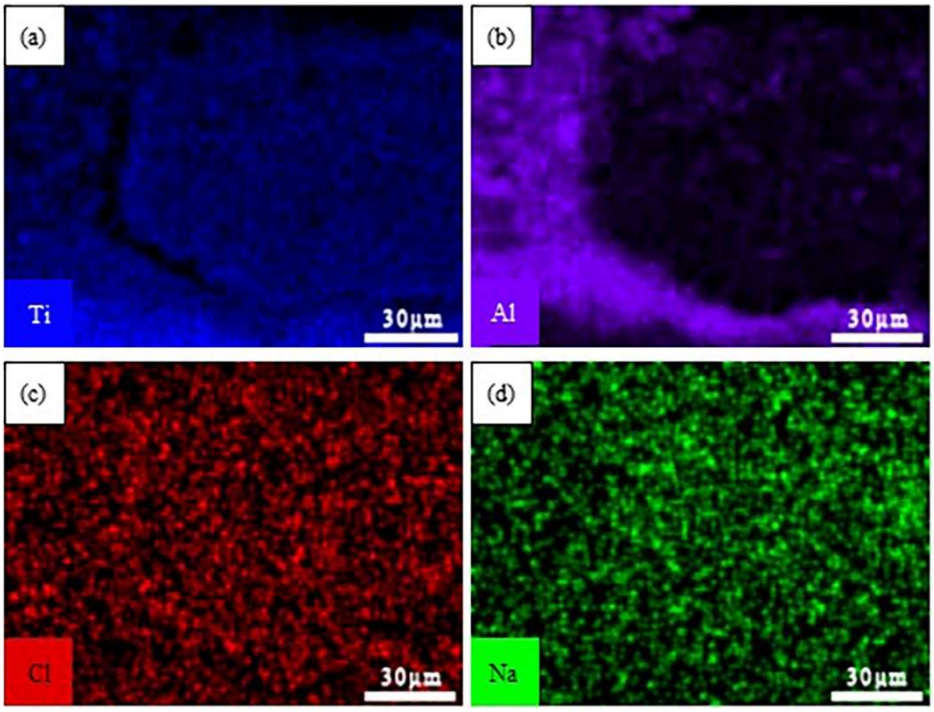

Figure 10. Element mappings of hot dip aluminum/carburizing composite coating (Ti, Al, Cl, Na are represented by blue, purple, red, and green respectively).

Table 4. EDS results of regions marked in Figure 9(b) (at.%).

Point	Ti	Al	O	Cl	Na	Possible phase
A	21.96	15.58	60.71	/	1.75	Al_2O_3+TiO_2
B	19.47	10.39	67.10	/	3.05	TiO_2+Na_2TiO_3
C	18.21	30.96	50.83	/	/	Al_2O_3+TiO_2
D	9.50	29.00	60.20	0.64	0.66	Al_2O_3+$TiAl_2$
E	34.33	65.57	/	/	/	$TiAl_2$
F	46.85	53.15	/	/	/	TiAl
G	80.36	19.64	/	/	/	Ti_3Al
Mean	32.95	32.06	59.71	0.64	0.92	/

4. Discussion

From the above-mentioned results, it can be clearly concluded that both hot dip aluminum composite coating and hot dip aluminum/carburizing composite coating can protect the Ti65 titanium alloys when exposed to a molten salt environment. The corrosion resistance of Ti-based alloy is not enhanced much by hot dip aluminum/carburizing composite coating but is improved significantly by hot dip aluminum coating.

4.1. The microstructures of the hot dip aluminum/carburizing composite coating

For hot dip aluminum coating, hot dip aluminum coating consists of $TiAl_3$ phase near the substrate and a mixed layer containing $TiAl_3$ and pure Al [20, 23]. Firstly, during the corrosion experiment, the Al and $TiAl_3$ could be firstly oxidized generating TiO_2 and Al_2O_3 as follows:

$$2Al+2/3O_2=Al_2O_3 \quad (2)$$

$$2TiAl_3+13/2O_2=2TiO_2+Al_2O_3 \quad (3)$$

 doi:10.20944/preprints202306.1311.v1

A layer of Ti-Al ($TiAl_2$ TiAl, Ti_3Al) also can be formed at the interface between the coating and Ti65 substrate, which is mainly due to the outward diffusion of Ti atoms from the substrate and the Al atoms diffused inwards during the corrosion process. The interfacial reaction can be illustrated as below:

$$TiAl_3+Ti=TiAl_2+TiAl \quad (4)$$

$$TiAl+2Ti=Ti_3Al \quad (5)$$

Ti-Al ($TiAl_2$, TiAl, Ti_3Al) layers were compact, uniform structures, which effectively blocked the penetration of the atoms/particles.

Given that the melting point of NaCl(s) is 801 ^{o}C, so NaCl salt keeps a melt state on the coating at the test temperature of 810 ^{o}C, leading to the dissolution of oxide scales as follows:

$$Al_2O_3+2NaCl+1/2O_2=2NaAlO_2+Cl_2 \quad (6)$$

$$TiO_2+2NaCl+1/2O_2=Na_2TiO_3+Cl_2 \quad (7)$$

However, no diffraction peaks of corrosion products $NaAlO_2$ and Na_2TiO_3 were detected in XRD results, indicating the content of $NaAlO_2$ and Na_2TiO_3 is relatively low. Besides, the corrosion products detected by XRD were mainly composed of $TiAl_3$, showing that the coating still presents an excellent corrosion resistance. More importantly, the reaction between $TiAl_3$ and O_2 can be considered as the main oxidation mechanism of hot dip aluminum coating in hot corrosion environments.

4.2. The microstructures of the hot dip aluminum/carburizing composite coating

For hot dip aluminum/carburizing composite coating, the molten salt corrosion products detected by XRD are mainly composed of Al_2O_3 and $TiAl_3$. During the initial stage of the hot corrosion test, the free carbon atoms in the outermost layer were oxidized, causing the formation of vacancy through the scale. These defects provided short-circuit diffusion channel for the inward diffusion of the corrosive medium, and thus contributed to accelerate the whole corrosion process. The reactions can be written as follows:

$$C+O_2=CO_2 \quad (8)$$

Subsequently, the oxygen and NaCl particles would gradually penetrate the coating. However, the initially formed TiO_2 would be promptly destroyed in the early stage of its emergence because of the attack of chloride ion exhibited porous structure, which could not protect the underlying coatings from corrosion[28], and the oxides generated on the coating surface could react with NaCl as follows:

$$Al_2O_3+2NaCl+1/2O_2=2NaAlO_2+Cl_2 \quad (6)$$

$$TiO_2+2NaCl+1/2O_2=Na_2TiO_3+Cl_2 \quad (7)$$

Na_2TiO_3 and $NaAlO_2$ were evidently detected in hot dip aluminum/carburizing composite coating based on XRD pattern (Figure 7(b)) and EDS results (Table 4). Besides, $Na_xTi_yO_z$ corrosion products have been reported to exhibit a porous structure and fail to protect the underlying coating from corrosion [29, 30]. On the other hand, growth stress and thermal stress were easily released for the porous structure[31]. The oxygen seeps further throng the porous structure leading to severe internal oxidation as follows:

$$TiC+O_2=TiO_2+CO^{[32]} \quad (9)$$

$$Al_4C_3+6O_2=2Al_2O_3+3CO_2 \quad (10)$$

$$2Ti_3AlC+7O_2=5TiO_2+TiAl_2+2CO_2 \quad (11)$$

$$2TiAl_3+13/2O_2=2TiO_2+3Al_2O_3 \quad (12)$$

$$4TiAl_3+3O_2=4TiAl_2+2Al_2O_3 \quad (13)$$

There are a high concentration of vacancy in the coating since the loss of C atoms. The reaction of newly formed Al_2O_3 can fill the defects improving the resistance to salt corrosion of coating. However, the presence of TiO_2 particles interrupted Al_2O_3 continuity, consequently resulting in the formation of loose and porous corrosion regions of TiO_2 with clear voids and micro-channel. Moreover, the chloride would pass through the vacancy and micro-channel dissolving the oxide scale as equations (6)(7).

In addition, with the molten salt corrosion time increasing, the oxide scales were continuously consumed, so that the Al content in the coating is insufficient to form Al_2O_3 scale. Once the reaction of equations (6) and (7) occurs, some of the resulting Cl_2 cross the metal/oxide or coating/oxide interface and reacts with Al and Ti. The reaction can be written as:

$$Al+3/2Cl_2=AlCl_3 \quad (14)$$

$$Ti+Cl_2=TiCl_2 \quad (15)$$

$$2/3Ti+Cl_2=2/3TiCl_3 \quad (16)$$

$$Ti+2Cl_2=TiCl_4 \quad (17)$$

The volatile chloride produced by the reaction will be diffused outward with the inward-diffused oxygen, which can be expressed as follows:

$$TiCl_2+O_2=TiO_2+Cl_2 \quad (18)$$

$$2TiCl_3+O_2=2TiO_2+3Cl_2 \quad (19)$$

$$TiCl_4+O_2=TiO_2+2Cl_2 \quad (20)$$

$$2AlCl_3+3/2O_2=Al_2O_3+3Cl_2 \quad (21)$$

In this way, gaseous Cl_2 is produced again, so the reaction process occurring in NaCl-covered hot dip aluminum/carburizing composite coatings can be regarded as the self-sustainable oxychlorination.

5. Conclusions

The composite coating of hot dip aluminum /carburizing composite coating was successfully prepared on Ti65 titanium alloy by a two-step method of hot dipping aluminum and solid carburizing. The intermetallic compound layer can be divided into two layers after aluminizing: the inner layer consisting mainly of Ti_3Al and the outer layer composed of granular $TiAl_3$ and a mixed layer of pure Al filled between particles. During the carburization process, aluminum elements continue to diffuse to the substrate and the titanium elements in the substrate continue to diffuse to the coating during carburization, forming a series of hot dip aluminum alloy layers ($TiAl_2$, TiAl, Ti_3Al) from the outside to the inside. The coating consists of compounds such as TiC, Al_4C_3, Ti_3AlC, and free carbon atoms. This results in the formation of a composite coating of hot dip aluminum /carburizing. According to their (Ti65 titanium alloy, hot dip aluminum coating corrosion, and hot dip aluminum/carburizing coating) corrosion behavior in NaCl salt, the following conclusions can be drawn:

(1) Both hot dip aluminum coating and hot dip aluminum/carburizing coating can effectively improve the corrosion resistance of sodium chloride molten salt. However, the hot dip aluminum coating exhibits superior corrosion resistance in NaCl salt at 810°C compared to the hot dip aluminum/carburizing coating.

(2) For hot dip aluminum coating, after molten salt corrosion for 120h, the outer layer mainly forms a mixture of $TiAl_3$, Al_2O_3, TiO_2, while the inner layer forms a layered structure of $TiAl_2$/TiAl/Ti_3Al. The mixture of $TiAl_3$ and Al_2O_3 in the outer layer plays a good protective role. In addition, the inner $TiAl_2$/TiAl/Ti_3Al was well bonded to the substrate, smooth and without cracking.

(3) For hot dip aluminum/carburizing composite coating, carbon exists in the coating as free carbon atoms, TiC, Ti_3AlC. During the process of molten salt corrosion, C is oxidized into CO_2 /CO gas, leading to the formation of high concentration vacancy in the coating, which becomes a channel for molten salt ions and oxygen to penetrate. In addition, TiC and Ti_3AlC promote the formation of non-protective oxide TiO_2, resulting in a deterioration of corrosion resistance and a self-catalytic corrosion mechanism.

(4) The coating after carburizing is beneficial to reduce the generation of cracks, because Al and Ti atoms also take place in the process of carburizing to form an Al-Ti binary alloy phase layer.

Author Contributions: Investigation, data curation, writing—original draft, J.W.; Supervision, funding acquisition, project administration, writing—review and editing F.L.. All authors have read and agreed to the published version of the manuscript.

Funding: This research was funded by Science and Technology Project of Education Department of Hunan Province (No. 22A0100), Hunan Provincial Natural Science Foundation of China (No. 2021JJ30672), and National Training Program for College Students' Innovation and Entrepreneurship (No. 202210530036).

Institutional Review Board Statement: Not applicable.

Informed Consent Statement: Not applicable.

Data Availability Statement: Not applicable.

Acknowledgments: The authors gratefully acknowledge the support provided by Materials Intelligent Design College Students' Innovation and Entrepreneurship Education Center, Xiangtan University, Xiangtan, Hunan, China.

Conflicts of Interest: The authors declare no conflict of interest.

Reference

1. Huang, L.; An, Q.; Geng, L.; Wang, S.; Jiang, S.; Cui, X.; Zhang, R.; Sun, F.; Jiao, Y.; Chen, X.; Wang, C. Multiscale Architecture and Superior High-Temperature Performance of Discontinuously Reinforced Titanium Matrix Composites. *Adv Mater.* **2021**, *33*, e2000688. https://dx.doi.org/10.1002/adma.202000688.
2. Li, B.; Zhou, H.; Liu, J.; Kang, C. Multiaxial fatigue damage and reliability assessment of aero-engine compressor blades made of TC4 titanium alloy. *Aerospace Science and Technology*. **2021**, *119*. https://dx.doi.org/10.1016/j.ast.2021.107107.
3. Singh, G.; Ramamurty, U. Reprint: Boron modified titanium alloys. *Progress in Materials Science*. **2021**, *120*. https://dx.doi.org/10.1016/j.pmatsci.2021.100815.
4. Sun, J.; Qi, M.; Zhang, J.; Li, X.; Wang, H.; Ma, Y.; Xu, D.; Lei, J.; Yang, R. Formation mechanism of α lamellae during $\beta \rightarrow \alpha$ transformation in polycrystalline dual-phase Ti alloys. *Journal of Materials Science & Technology*. **2021**, *71*, 98-108. https://dx.doi.org/10.1016/j.jmst.2020.02.093.
5. Zhang, X.; Chen, Y.; Hu, J. Recent advances in the development of aerospace materials. *Progress in Aerospace Sciences*. **2018**, *97*, 22-34. https://dx.doi.org/10.1016/j.paerosci.2018.01.001.
6. Ciszak, C.; Popa, I.; Brossard, J.-M.; Monceau, D.; Chevalier, S. NaCl induced corrosion of Ti-6Al-4V alloy at high temperature. *Corrosion Science*. **2016**, *110*, 91-104. https://dx.doi.org/10.1016/j.corsci.2016.04.016.
7. Fan, L.; Liu, L.; Cui, Y.; Cao, M.; Yu, Z.; Oguzie, E.E.; Li, Y.; Wang, F. Effect of streaming water vapor on the corrosion behavior of Ti60 alloy under a solid NaCl deposit in water vapor at 600 °C. *Corrosion Science*. **2019**, *160*. https://dx.doi.org/10.1016/j.corsci.2019.108177.
8. Li, R.; Liu, L.; Cui, Y.; Liu, R.; Fan, L.; Cao, M.; Yu, Z.; Chen, Z.; Wang, Q.; Wang, F. Corrosion behavior of Ti60 alloy under continuous NaCl solution spraying at 600 °C. *Journal of Materials Science & Technology*. **2022**, *124*, 86-101. https://dx.doi.org/10.1016/j.jmst.2022.01.032.
9. Z. Yao, M.M. NaCl-induced hot corrosion of a titanium aluminide alloy *Materials Science and Engineering A*. **1995**, *192/193* 6.

10. Rubacha, K.; Godlewska, E.; Mars, K. Behaviour of a silicon-rich coating on Ti-46Al-8Ta (at.%) in hot-corrosion environments. *Corrosion Science.* **2017**, *118*, 158-167. https://dx.doi.org/10.1016/j.corsci.2017.02.002.
11. Wu, L.-K.; Wu, J.-J.; Wu, W.-Y.; Yan, H.-J.; Jiang, M.-Y.; Cao, F.-H. Hot corrosion behavior of electrodeposited SiO2 coating on TiAl alloy. *Corrosion Science.* **2020**, *174*. https://dx.doi.org/10.1016/j.corsci.2020.108827.
12. Hu, Y.-t.; Zheng, L.; Yan, H.-j.; Wu, L.-k.; Lin, X.-j.; Cao, F.-h.; Jiang, M.-y. Improving hot corrosion resistance of aluminized TiAl alloy by anodization and pre-oxidation. *Transactions of Nonferrous Metals Society of China.* **2021**, *31*, 193-206. https://dx.doi.org/10.1016/s1003-6326(20)65487-5.
13. Zhang, M.; Liang, Y.; Feng, M.; Jiang, C.; Zhang, Y.; Wang, Y.; Feng, Y.; Ma, L.; Wang, F. Corrosion behaviour of aluminide coatings on Ti-based alloy in the marine environment at high temperature. *Corrosion Science.* **2022**, *209*. https://dx.doi.org/10.1016/j.corsci.2022.110750.
14. Zhaolin Tang *, F.W., Weitao Wu. <14.pdf>. *Materials Science and Engineering A.* **2000**, *276*.
15. Huilgol, P.; Udupa, K.R.; Bhat, K.U. Metastable microstructures at the interface between AISI 321 steel and molten aluminum during hot-dip aluminizing. *Surface and Coatings Technology.* **2018**, *348*, 22-30. https://dx.doi.org/10.1016/j.surfcoat.2018.05.013.
16. Shao, Z.; Yang, H.; Zhang, S.; Liu, W.; Xiao, Z.; Zheng, M. A dense Fe-Al/Al2O3 coating as tritium permeation barrier on CLAM steel by hot-dipping aluminizing. *Surface and Coatings Technology.* **2022**, *440*. https://dx.doi.org/10.1016/j.surfcoat.2022.128491.
17. Shibli, S.M.A.; Manu, R.; Dilimon, V.S. Effect of nickel-rich barrier layer on improvement of hot-dip zinc coating. *Applied Surface Science.* **2005**, *245*, 179-185. https://dx.doi.org/10.1016/j.apsusc.2004.10.007.
18. Patel, P.; Jamnapara, N.I.; Zala, A.; Kahar, S.D. Investigation of hot-dip aluminized Ti6Al4V alloy processed by different thermal treatments in an oxidizing atmosphere. *Surface and Coatings Technology.* **2020**, *385*. https://dx.doi.org/10.1016/j.surfcoat.2019.125323.
19. Wang, Y.; Xiong, J.; Yan, J.; Fan, H.; Wang, J. Oxidation resistance and corrosion behavior of hot-dip aluminized coatings on commercial-purity titanium. *Surface and Coatings Technology.* **2011**, *206*, 1277-1282. https://dx.doi.org/10.1016/j.surfcoat.2011.08.042.
20. Jeng, S.-C. Oxidation behavior and microstructural evolution of hot-dipped aluminum coating on Ti-6Al-4V alloy at 800°C. *Surface and Coatings Technology.* **2013**, *235*, 867-874. https://dx.doi.org/10.1016/j.surfcoat.2013.09.023.
21. Duan, H.-q.; Han, Y.-f.; LÜ, W.-j.; Mao, J.-w.; Wang, L.-q.; Zhang, D. Effect of solid carburization on surface microstructure and hardness of Ti-6Al-4V alloy and (TiB+La2O3)/Ti-6Al-4V composite. *Transactions of Nonferrous Metals Society of China.* **2016**, *26*, 1871-1877. https://dx.doi.org/10.1016/s1003-6326(16)64301-7.
22. Liao, C.; Yang, J.; He, Y.; Ming, X. Electrochemical corrosion behavior of the carburized porous TiAl alloy. *Journal of Alloys and Compounds.* **2015**, *619*, 221-227. https://dx.doi.org/10.1016/j.jallcom.2014.08.021.
23. Yao, T.; Liu, Y.; Liu, B.; Song, M.; Zhao, K.; Zhang, W.; He, Y. Influence of carburization on oxidation behavior of High Nb contained TiAl alloy. *Surface and Coatings Technology.* **2015**, *277*, 210-215. https://dx.doi.org/10.1016/j.surfcoat.2015.07.058.
24. Wohlert, S.; Bormann, R. Phase selection governed by different growth velocities in the early stages of the Ti/Al phase reaction. *J. Appl. Phys.* **1999**, *85*, 825-832, <Go to ISI>://WOS:000077792600028.
25. Hsu, I.C.; Wu, S.K.; Lin, R.Y. A study of aluminum cladding on Ti50Al50 intermetallics by liquid aluminizing. *Materials Chemistry and Physics.* **1997**, *49*, 184-190. https://dx.doi.org/10.1016/s0254-0584(97)01892-0.
26. Jiang, S.-y.; Li, S.-c.; Zhang, L. Microstructure evolution of Al–Ti liquid–solid interface. *Transactions of Nonferrous Metals Society of China.* **2013**, *23*, 3545-3552. https://dx.doi.org/10.1016/s1003-6326(13)62899-x.
27. Alam, M.Z.; Das, D.K. Effect of cracking in diffusion aluminide coatings on their cyclic oxidation performance on Ti-based IMI-834 alloy. *Corrosion Science.* **2009**, *51*, 1405-1412. https://dx.doi.org/10.1016/j.corsci.2009.03.027.
28. Ciszak, C.; Abdallah, I.; Popa, I.; Brossard, J.-M.; Vande Put, A.; Monceau, D.; Chevalier, S. Degradation mechanism of Ti-6Al-2Sn-4Zr-2Mo-Si alloy exposed to solid NaCl deposit at high temperature. *Corrosion Science.* **2020**, *172*. https://dx.doi.org/10.1016/j.corsci.2020.108611.
29. Wang, Z.; Ma, G.; Li, Z.; Ruan, H.; Yuan, J.; Wang, L.; Ke, P.; Wang, A. Corrosion mechanism of Ti2AlC MAX phase coatings under the synergistic effects of water vapor and solid NaCl at 600 °C. *Corrosion Science.* **2021**, *192*. https://dx.doi.org/10.1016/j.corsci.2021.109788.
30. Li, R.; Wang, S.; Zhou, D.; Pu, J.; Yu, M.; Guo, W. A new insight into the NaCl-induced hot corrosion mechanism of TiN coatings at 500 °C. *Corrosion Science.* **2020**, *174*. https://dx.doi.org/10.1016/j.corsci.2020.108794.
31. Chang, L.M.; Liu, J.H.; Zhang, R.J. Corrosion behaviour of electrodeposited Ni/Al2O3 composite coating covered with a NaCl salt film at 800 degrees C. *Materials and Corrosion-Werkstoffe Und Korrosion.* **2011**, *62*, 920-925. https://dx.doi.org/10.1002/maco.200905617.

32. Chen, L.; Zhang, X.; Wu, Y.; Chen, C.; Li, Y.; Zhou, W.; Ren, X. Effect of surface morphology and microstructure on the hot corrosion behavior of TiC/IN625 coatings prepared by extreme high-speed laser cladding. *Corrosion Science.* **2022**, *201*. https://dx.doi.org/10.1016/j.corsci.2022.110271.